Structural and functional analysis of an essential nucleoporin heterotrimer on the cytoplasmic face of the nuclear pore complex

Kimihisa Yoshida, Hyuk-Soo Seo, Erik W. Debler, Günter Blobel[1], and André Hoelz[1,2]

Laboratory of Cell Biology, Howard Hughes Medical Institute, The Rockefeller University, 1230 York Avenue, New York, NY 10065

Contributed by Günter Blobel, August 15, 2011 (sent for review August 1, 2011)

So far, only a few of the interactions between the ≈30 nucleoporins comprising the modular structure of the nuclear pore complex have been defined at atomic resolution. Here we report the crystal structure, at 2.6 Å resolution, of a heterotrimeric complex, composed of fragments of three cytoplasmically oriented nucleoporins of yeast: Nup82, Nup116, and Nup159. Our data show that the Nup82 fragment, representing more than the N-terminal half of the molecule, folds into an extensively decorated, seven-bladed β-propeller that forms the centerpiece of this heterotrimeric complex and anchors both a C-terminal fragment of Nup116 and the C-terminal tail of Nup159. Binding between Nup116 and Nup82 is mutually reinforced via two loops, one emanating from the Nup82 β-propeller and the other one from the β-sandwich fold of Nup116, each contacting binding pockets in their counterparts. The Nup82-Nup159 interaction occurs through an amphipathic α-helix of Nup159, which is cradled in a large hydrophobic groove that is generated from several large surface decorations of the Nup82 β-propeller. Although Nup159 and Nup116 fragments bind to the Nup82 β-propeller in close vicinity, there are no direct contacts between them, consistent with the noncooperative binding that was detected biochemically. Extensive mutagenesis delineated hot-spot residues for these interactions. We also showed that the Nup82 β-propeller binds to other yeast Nup116 family members, Nup145N, Nup100 and to the mammalian homolog, Nup98. Notably, each of the three nucleoporins contains additional nuclear pore complex binding sites, distinct from those that were defined here in the heterotrimeric Nup82•Nup159•Nup116 complex.

assembly | evolutionary conservation | nucleo-cytoplasmic transport | site-directed mutagenesis | X-ray crystallography

Following the discovery of the nuclear pore complex (NPC) in the 1950s, numerous electron microscopic studies since have refined our understanding of its architecture to a resolution in the upper single-digit nanometer range (1). Collectively, these studies showed that NPCs are embedded in ≈100 nm wide circular openings, resulting from a circumscribed fusion of the double membrane of the nuclear envelope. The NPC consists of a symmetric central core and asymmetric filament-like structures that project to the nucleoplasmic and cytoplasmic sides. The core of the NPC displays a twofold axis of symmetry in the plane of the membrane and an eightfold rotational symmetry in the nucleocytoplasmic direction. As observed by cryoelectron tomography, the NPC can undergo huge structural changes (2) that remain to be characterized at the atomic level.

Beginning in the 1980s, biochemical and genetic analyses of the NPC and its surrounding pore membrane domain of the nuclear envelope has yielded an inventory consisting of ≈30 distinct NPC proteins termed nups (for nucleoporins) and of three distinct integral membrane proteins termed poms (for pore membrane proteins) that anchor the NPC. "Asymmetric" nups make up the filament-like structures on either side of the symmetric core and occur in at least eight copies, whereas "symmetric" nups in the core occur in at least 16 copies (1).

Nups consist of a combination of unstructured regions and standard structural folds, such as β-propellers, α-helical solenoids, and coiled coils (1). Many of the unstructured regions are marked by repetitive Phe-Gly motifs and were therefore dubbed FG-repeat regions. Such regions occur in both symmetric and asymmetric nups. Early on, FG repeats were identified as docking sites for a collection of various transport factors that in turn recognize signals on substrates for nuclear import and export (3, 4). Several of the asymmetric nups also contain binding sites for enzymes and other proteins involved in nucleo-cytoplasmic transport. The local concentrations of these enzymes and proteins on either side of the NPC are among the determinants for directionality of transport to either the nucleus or the cytoplasm. Several of these binding sites have already been characterized at the atomic level. Moreover, some crystallographic analyses of the extensive nucleoporin interactome, especially of the symmetric core, have been reported (1).

In order to gain deeper insight into the structure of the cytoplasmic filament network of the yeast *Saccharomyces cerevisiae* NPC, we assembled a heterotrimeric complex from fragments comprising more than the N-terminal half of Nup82, the C-terminal domain of Nup116, and the C-terminal tail of Nup159. We present the crystal structure of this heterotrimer, carried out extensive structure-guided mutagenesis to identify hot-spot residues for these interactions, and showed that the interacting sites have been highly conserved in evolution.

Results

Assembly of a Nup82^{NTD}•Nup159^{T}•Nup116^{CTD} Heterotrimer. A domain structure for each of three cytoplasmically exposed nucleoporins of *S. cerevisiae*, Nup82, Nup159, and Nup116, is shown in Fig. 1*A* (1, 5–12). It was previously reported that full-length Nup82 reacts in an overlay blot with a C-terminal fragment of Nup159, Nup159$^{1223–1460}$ (7). In further narrowing down the size of interacting domains, we found that an N-terminal fragment of Nup82, Nup82$^{1–452}$, (referred to as the Nup82 N-terminal domain, Nup82^{NTD}) and the C-terminal tail of Nup159 (Nup159$^{1425–1460}$, Nup159^{T}) formed a 1:1 complex with a molar mass of 58 kDa, as determined by size exclusion chromatography combined with multiangle light scattering (Fig. 1*B*). However, this complex failed to crystallize, perhaps because of an unsaturated binding site. A candidate for a missing binding partner was the C-terminal

Author contributions: K.Y., H.-S.S., E.W.D., G.B., and A.H. designed research; K.Y., H.-S.S., E.W.D., and A.H. performed research; K.Y., H.-S.S., E.W.D., G.B., and A.H. analyzed data; and K.Y., H.-S.S., E.W.D., G.B., and A.H. wrote the paper.

The authors declare no conflict of interest.

Data deposition: The atomic coordinates have been deposited in the Protein Data Bank, www.pdb.org (PDB ID code 3PBP).

[1]To whom correspondence may be addressed. E-mail: blobel@rockefeller.edu or hoelz@caltech.edu.

[2]Present address: California Institute of Technology, Division of Chemistry and Chemical Engineering, 1200 East California Boulevard, Pasadena, CA 91125.

This article contains supporting information online at www.pnas.org/lookup/suppl/doi:10.1073/pnas.1112846108/-/DCSupplemental.

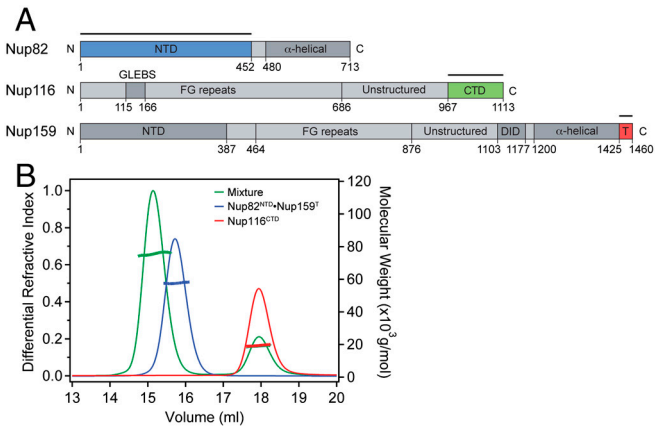

Fig. 1. Assembly of a Nup82^{NTD}•Nup159^{T}•Nup116^{CTD} heterotrimer. (*A*) Domain organization of yeast Nup82, Nup116, and Nup159 (1). Bars denote the fragments that were used for heterotrimer assembly and crystallization: Nup82 N-terminal domain (NTD, blue); Nup116 C-terminal domain (CTD, green); and Nup159 C-terminal tail (T, red). GLEBS, binding site for the RNA export factor Gle2; DID, dynein light chain interacting domain. (*B*) Analysis by size exclusion chromatography coupled to multiangle light scattering. The differential refractive indices of Nup116^{CTD} (red), Nup82^{NTD}•Nup159^{T} (blue), and Nup82^{NTD}•Nup159^{T}•Nup116^{CTD} (green) are plotted against the elution volumes from a Superdex 200 10/300 GL gel filtration column (GE Healthcare) with dots indicating molar masses.

region of Nup116 that had previously been reported to interact with N-terminal fragments of Nup82 in a yeast two-hybrid system (13); furthermore, the solution structure of the C-terminal region of Nup116 (Nup116$^{967–1113}$, referred to as Nup116^{CTD}) had already been solved by NMR (14). Indeed, we were able to assemble a soluble 1:1:1 Nup82^{NTD}•Nup159^{T}•Nup116^{CTD} heterotrimer with a molar mass of 76 kDa, as determined by size exclusion chromatography combined with multiangle light scattering (Fig. 1*B*), and we found that this complex crystallized.

Structure Determination of the Heterotrimer. The Nup82^{NTD}•Nup159^{T}•Nup116^{CTD} heterotrimer crystallized in space group P1 with four trimeric complexes in the asymmetric unit. The structure was solved by single anomalous dispersion (SAD) using X-ray diffraction data of seleno-L-methionine-labeled crystals and was refined to a resolution of 2.6 Å with R_{free} and R_{work} values of 27.2% and 25.7%, respectively. For details of data collection and refinement statistics, see Table 1. The four heterotrimers in the asymmetric unit align with a root-mean square deviation of ≈0.5 Å, suggesting limited conformational flexibility. Because there was no evidence that the heterotrimer formed higher-order structures in solution, we focused our structural analyses on the Nup82^{NTD}•Nup159^{T}•Nup116^{CTD} heterotrimer.

Individual Components of the Heterotrimer. The heterotrimer forms an irregular structure of ≈90 Å × 60 Å × 50 Å and is shown in different orientations in Fig. 2 *A–C*. The polypeptide chain of Nup82^{NTD} folds into a seven-bladed β-propeller and lacks a Velcro closure that typically intertwines blades 1 and 7 by providing a forth β-strand to the terminal seventh blade (15). Instead, a short extension at the N terminus links blades 1 and 7 by forming several hydrophobic contacts and hydrogen bonds with both blades (Fig. 2 *C* and *D*). The β-propeller contains numerous surface decorations consisting of α-helices, β-strands, and loops indicated in the schematic ribbon model of Fig. 2*D*.

Nup116^{CTD} folds into a β-sandwich with numerous protruding loops and is flanked at each end by an α-helix, termed αA and αB (Fig. S1). One of the two β-sheets is formed by six antiparallel β-strands, while the opposing β-sheet contains only two antiparallel β-strands, resulting in a groove on the molecular surface between helix αB and strand β5 (Figs. S1 and S2). This β-sandwich

Table 1. Crystallographic analysis

	SeMet SAD
Data collection	
Synchrotron	APS*
Beamline	GM/CA-CAT 23ID-B
Space group	P1
Cell dimensions	
a, *b*, *c* (Å)	$a = 61.5$, $b = 96.8$, $c = 144.3$
α, β, γ (°)	$\alpha = 106.0$, $\beta = 94.0$, $\gamma = 108.2$
Wavelength (Å)	0.9794 (*Se Peak*)
Resolution (Å)†	50.0-2.6 (2.69-2.60)
R_{sym} (%)†	9.7 (47.3)
$\langle I/\sigma I \rangle$†	11.0 (3.0)
Completeness (%)†	98.8 (98.3)
Redundancy†	2.0 (2.0)
Refinement	
Resolution (Å)	50.0-2.6
No. reflections	168,608
Test set	14,690 (8.0 %)
R_{work}/R_{free} (%)	25.7/27.2
No. of atoms	19,661
rms deviations	
Bond angles (°)	1.4
Bond lengths (Å)	0.008
Ramachandran statistics‡	
Most favored (%)	83.4
Additionally allowed (%)	15.7
Generously allowed (%)	0.9
Disallowed (%)	0.0

*APS, Advanced Photon Source, Argonne National Laboratory.
†Highest-resolution shell is shown in parentheses.
‡As determined by Procheck (28).

fold was first reported in the crystal structures of human Nup98$^{721–863}$ and of *S. cerevisiae* Nup145N$^{443–605}$ (16, 17), as well as in the NMR structure of Nup116^{CTD} (14). A prominent feature of Nup116^{CTD} is the 19-residue loop between β6 and αB that is critical for the interaction with Nup82^{NTD}. Finally, Nup159^{T} forms a 26-residue amphipathic α-helix that binds in a surface groove at the lower edge of the Nup82 β-propeller (Fig. 2).

Heterotrimer Interfaces. The Nup82-Nup116 interface is bipartite. Two loops, one emanating from the Nup82 β-propeller and one from the Nup116 β-sandwich, mediate the interaction with distinct pockets on their counterparts. One of these loops, the 3D4A loop of Nup82, binds with a Phe-Gly-Leu (FGL) motif located at its tip to the prominent hydrophobic groove on the Nup116 surface (Fig. 3*A*, Fig. S2); we therefore refer to this loop as the "FGL loop." The other loop, the β6-αB loop of Nup116, binds with a distinct lysine residue to a Nup82 pocket, located at the side of the β-propeller (Fig. 3*B*, Fig. S3); we therefore refer to this loop as the "K-loop." A salient feature of this interaction is a salt bridge between the invariant lysine residue of Nup116 (K1063) and an aspartate residue at the bottom of a Nup82 pocket (D204). This electrostatic interaction is reinforced by a hydrophobic bracelet formed by I287, F290, and Y295, located in the noncanonical insertion in the 4D5A connection of Nup82, and wrapping around the apolar base of the side chain of K1063 (Fig. 3*B*, Fig. S3). The two sites are adjacent and form an interface with a combined buried surface area of ≈1,740 Å^2 (Figs. S2 and S3).

The Nup82-Nup159 interface is characterized by the amphipathic α-helix of Nup159^{T} that is situated in a large groove of the Nup82 β-propeller, created by the exposed strands of blade 5 and the 4CD and 6CD helical insertions (Figs. 2*D* and 3*C*). Altogether, a combined surface area of ≈1,700 Å^2 is buried

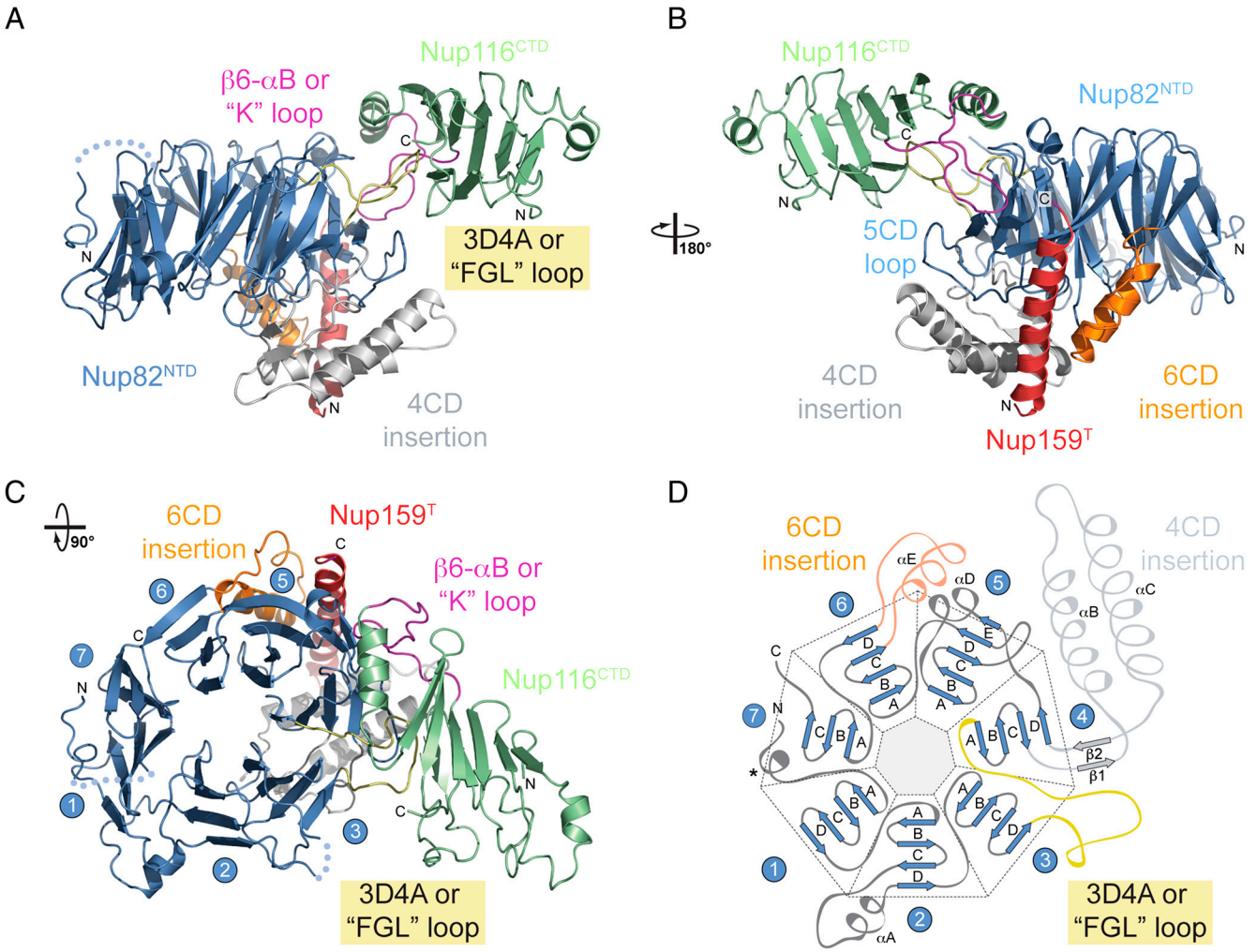

Fig. 2. Structural overview of the Nup82^{NTD}•Nup159^{T}•Nup116^{CTD} complex. (*A–C*) Ribbon representation from various angles. Nup82^{NTD} (blue) folds into a β-propeller with various noncanonical insertions highlighted in yellow (3D4A or "FGL" loop), gray (4CD), and orange (6CD); Nup116^{CTD} (green) is a β-sandwich with a β6-αB connector ("K-loop") indicated in magenta; Nup159^{T} (red) folds into an amphipathic α-helix. Dotted lines represent disordered regions. (*D*) Schematic representation of the β-propeller of Nup82^{NTD}. Prominent insertions and secondary structure elements are labeled. The asterisk denotes the N-terminal region that fits into the crevice between blades 1 and 7, replacing the canonical Velcro closure observed in most β-propellers.

between the two proteins, involving numerous, primarily hydrophobic residues (Figs. S3 and S4).

Paralogs and Orthologs of Nup116. While yeast Nup116 has two paralogs, Nup100 and Nup145N, only one ortholog exists in humans (hNup98). Both Nup145N and hNup98 are auto-proteolytic cleavage products of larger polypeptide chains, encompassing the N-terminal Nup145N or hNup98, followed by Nup145C or hNup96, respectively (18–20). Notably, hNup98 is also synthesized from an alternatively spliced mRNA that encodes for a

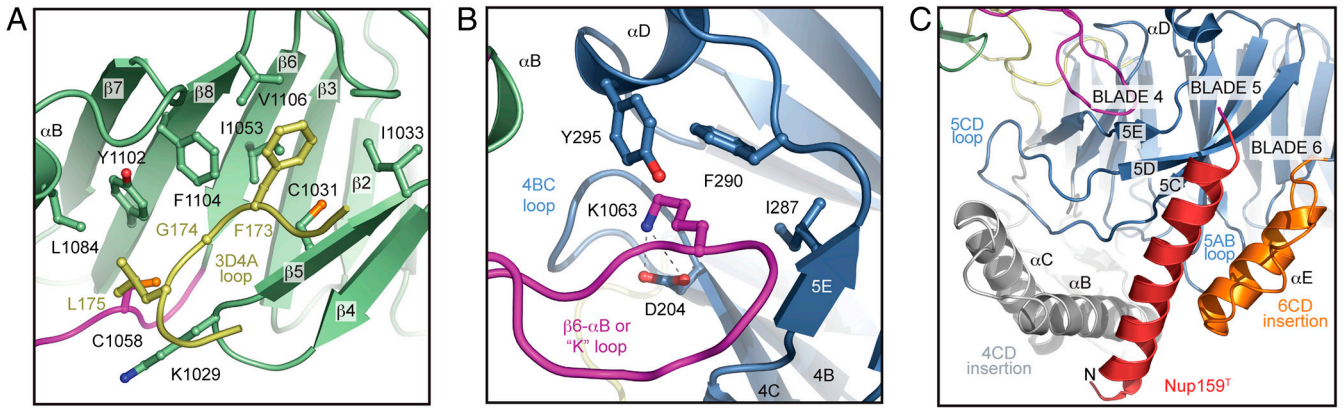

Fig. 3. Close-up view of the Nup82-Nup116 and Nup82-Nup159 interfaces. Nup82^{NTD} interacts with Nup116^{CTD} via two adjacent sites. (*A*) One site is formed by the 3D4A "FGL loop" of Nup82^{NTD}, which binds to a groove of Nup116^{CTD} between helix αB and strand β5. (*B*) The other site is formed by the "K-loop" of Nup116^{CTD}, K1063 of which binds to a Nup82 pocket with an aspartate (D204) at its bottom and a hydrophobic bracelet at its entry. (*C*) Nup159^{T} binds to a groove in Nup82^{NTD} that is formed by the 4CD and 6CD insertions and blade 5. Color code as in Fig. 2.

C-terminal 6-kDa protein instead of hNup96 (19). Auto-proteolytic cleavage at HF ↓ SKYGL requires a catalytic serine (18) that is not conserved in the Nup116 and Nup100 paralogs (Fig. S5).

The CTDs of Nup116 and hNup98 superpose with a root-mean square deviation of ≈2.0 Å. Strikingly, the binding of the FGL loop of Nup82^{NTD} to the groove of Nup116^{CTD} mimics the interaction of the Tyr-Gly-Leu (YGL) portion of the auto-proteolytic cleavage motif HF ↓ SKYGL bound to hNup98 (Fig. S1 *A* and *D*). To directly test the mimicry of these interactions, we utilized a construct (19) encoding hNup98^{CTD} and a C-terminal 6-kDa peptide (Fig. 4*A*), yielding an hNup98^{CTD}•6-kDa heterodimer composed of the auto-proteolytic cleavage products (Fig. 4 *B* and *C*). When this human heterodimer was mixed with the yeast Nup82^{NTD}•Nup159^{T} pair, a chimeric Nup82^{NTD}•Nup159^{T}•hNup98^{CTD} heterotrimer was formed displacing and releasing the 6-kDa peptide (Fig. 4 *B* and *C*). We showed that the other two Nup116 paralogs, Nup100 and Nup145N, also form heterotrimeric complexes with Nup82^{NTD}•Nup159^{T} (Fig. 5 *A* and *B*).

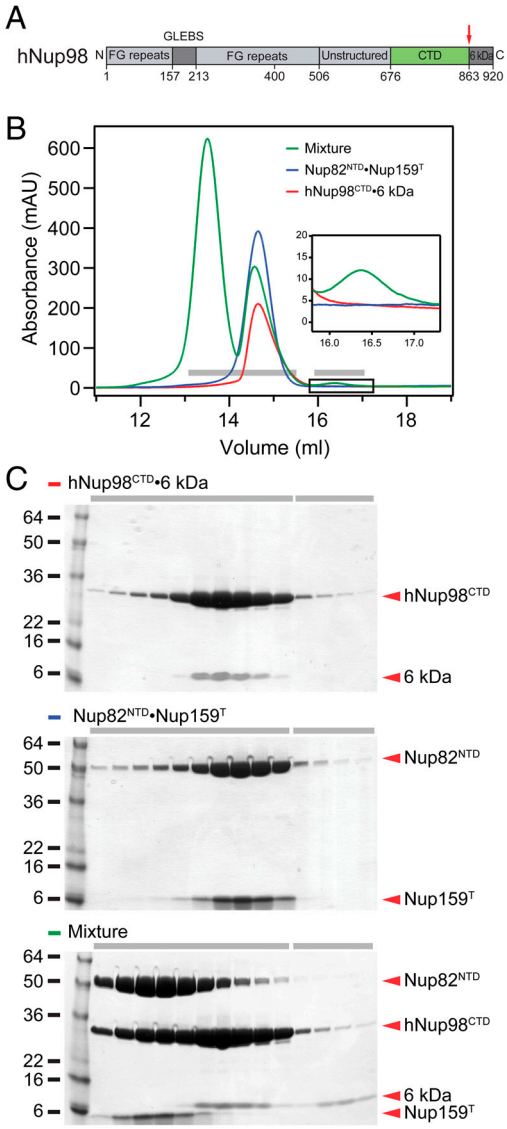

Fig. 4. Human Nup98^{CTD} binds to yeast Nup82^{NTD}. (*A*) Domain organization of human Nup98 (1, 18) indicating the C-terminal domain (CTD, green) and the auto-proteolytic 6-kDa protein (gray), as well as the auto-proteolytic cleavage site (red arrow). (*B*) Size exclusion chromatography analysis of purified yeast Nup82^{NTD}•Nup159^{T} (blue), human Nup98^{CTD}•6-kDa (red) and a mixture (green) in an ≈1:2 ratio. Note formation of a trimeric Nup82^{NTD}•Nup159^{T}•hNup98^{CTD} complex leads to displacement of the 6-kDa protein (inset). (*C*) Fractions, indicated by gray bars in (*B*), of hNup98^{CTD}•6-kDa (top), Nup82^{NTD}•Nup159^{T} (center), and their mixture (bottom) were analyzed by SDS-PAGE; proteins are indicated on the right and molecular weight standards on the left.

Mutational Analyses. To identify residues critical for mediating Nup82^{NTD}•Nup159^{T}•Nup116^{CTD} heterotrimer formation, we employed structure-guided mutagenesis and probed the mutants for complex formation by size exclusion chromatography (Table 2). For the interaction between Nup116^{CTD} and the Nup82^{NTD}•Nup159^{T} pair, we identified K1063 in the K-loop of Nup116^{CTD} as a hot-spot residue that, when mutated to alanine, abolished complex formation. By contrast, mutating D204, which forms a salt bridge with K1063, to alanine had only a mild effect on complex formation. However, the introduction of additional mutations, F290A and Y295A, at the entry of the hydrophobic pocket disrupted complex formation (Figs. S3 and S4). We refer to this mutant as Nup82^{DFY}. As measured by isothermal titration calorimetry (ITC), the deletion of the FGL loop in Nup82^{NTD} merely resulted in fivefold reduction in binding affinity to Nup116^{CTD} (Fig. S6 *A* and *B*), thus rendering the K-loop of Nup116^{CTD} the principal determinant for the Nup82^{NTD}-Nup116^{CTD} interaction.

To probe the Nup82^{NTD}-Nup159^{T} interaction, we mutated five large hydrophobic residues located in the 6CD insertion of the Nup82 β-propeller to alanine (Figs. S3 and S4). While the individual mutations of L393, I397, L402, L405, and F410 had no detectable effect (Table 2), their combination abolished complex formation. We refer to this mutant as Nup82^{LILLF}. As expected from the crystal structure, binding of Nup82^{LILLF} to Nup116^{CTD}

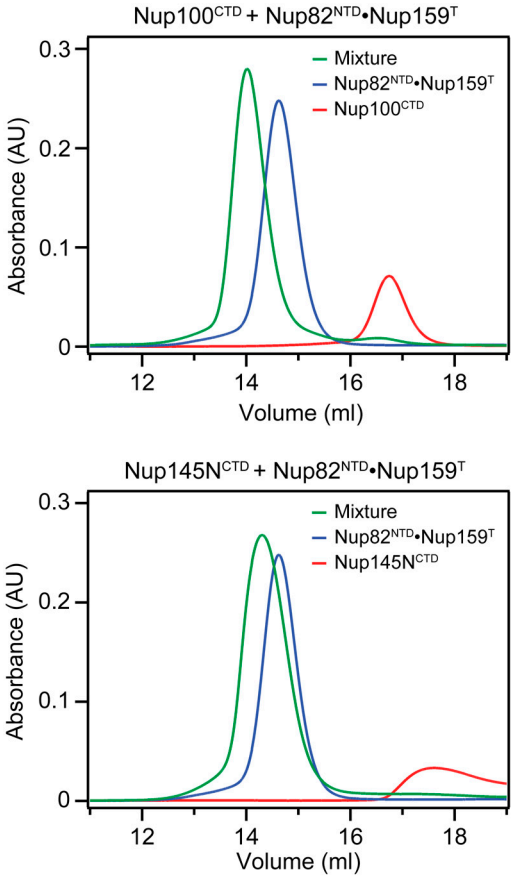

Fig. 5. Binding of yeast paralogs of Nup116^{CTD} to Nup82^{NTD}. Interaction analysis between Nup82^{NTD} • Nup159^{T} and the yeast Nup116^{CTD} homologs (*A*) Nup100^{CTD} and (*B*) Nup145N^{CTD}. Size exclusion chromatography analysis of Nup82^{NTD}•Nup159^{T} (blue), Nup100^{CTD} (red) and Nup145N^{CTD} (red), and their mixtures (green).

Table 2. Biochemical interaction analysis

$Nup82^{NTD}$ or $Nup82^{NTD}$•$Nup159^{T}$	Mutations *	Binding partner	Mutation	Relative binding†
$Nup82^{NTD}$•$Nup159^{T}$	wt	$Nup116^{CTD}$	wt	+++
$Nup82^{NTD}$•$Nup159^{T}$	Δ3D4A	$Nup116^{CTD}$	wt	+++
$Nup82^{NTD}$•$Nup159^{T}$	wt	$Nup116^{CTD}$	K1063A	-
$Nup82^{NTD}$•$Nup159^{T}$	D204A	$Nup116^{CTD}$	wt	++
$Nup82^{NTD}$•$Nup159^{T}$	F290A	$Nup116^{CTD}$	wt	++
$Nup82^{NTD}$•$Nup159^{T}$	Y295A	$Nup116^{CTD}$	wt	++
$Nup82^{NTD}$•$Nup159^{T}$	DFY	$Nup116^{CTD}$	wt	-
$Nup82^{NTD}$	L393A	$Nup159^{T}$‡	wt	+++
$Nup82^{NTD}$	I397A	$Nup159^{T}$	wt	+++
$Nup82^{NTD}$	L402A	$Nup159^{T}$	wt	+++
$Nup82^{NTD}$	L405A	$Nup159^{T}$	wt	+++
$Nup82^{NTD}$	F410A	$Nup159^{T}$	wt	+++
$Nup82^{NTD}$	LILLF	$Nup159^{T}$	wt	-
$Nup82^{NTD}$	DFY	$Nup159^{T}$	wt	+++
$Nup82^{NTD}$	LILLF	$Nup116^{CTD}$	wt	+++
$Nup82^{NTD}$	DFY-LILLF	$Nup159^{T}$	wt	-
$Nup82^{NTD}$	DFY-LILLF	$Nup116^{CTD}$	wt	-
$Nup82^{NTD}$•$Nup159^{T}$	wt	$Nup100^{CTD}$	wt	+++
$Nup82^{NTD}$•$Nup159^{T}$	DFY	$Nup100^{CTD}$	wt	-
$Nup82^{NTD}$•$Nup159^{T}$	wt	$Nup100^{CTD}$	K910A	-
$Nup82^{NTD}$•$Nup159^{T}$	wt	$Nup145N^{CTD}$	wt	+++
$Nup82^{NTD}$•$Nup159^{T}$	DFY	$Nup145N^{CTD}$	wt	-
$Nup82^{NTD}$•$Nup159^{T}$	wt	$Nup145N^{CTD}$	K558A	-
$Nup82^{NTD}$•$Nup159^{T}$	wt	$Nup98^{CTD}$	wt	+++
$Nup82^{NTD}$•$Nup159^{T}$	DFY	$Nup98^{CTD}$	wt	-
$Nup82^{NTD}$•$Nup159^{T}$	wt	$Nup98^{CTD}$	K814A	-

*$Nup82^{NTD}$ carries the C396S mutation, referred to as wild-type (wt).
†Relative binding was estimated in size exclusion chromatography from wild type-like binding (+++) to no detectable binding (–).
‡$Nup159^{T}$ binding experiments were carried out with a His_6-SUMO-$Nup159^{T}$ fusion protein.

was not affected and, vice versa, $Nup82^{DFY}$ retained binding to $Nup159^{T}$. The combination of these mutations in the $Nup82^{DFY-LILLF}$ variant resulted in loss of binding to both $Nup116^{CTD}$ and $Nup159^{T}$. These results are in accord with ITC data that revealed comparable affinities of $Nup82^{NTD}$ for $Nup116^{CTD}$ in the presence and absence of $Nup159^{T}$ [dissociation constants (K_d) of ≈50 and ≈60 nM, respectively] (Fig. S6 *A* and *C*). We conclude that $Nup82^{NTD}$ facilitates noncooperative binding to $Nup159^{T}$ and $Nup116^{CTD}$.

Based on our result that the CTDs of the Nup116 family members Nup100, Nup145N, and hNup98 interact with $Nup82^{NTD}$•$Nup159^{T}$, we tested whether the identified mutations would also abolish complex formation with these proteins. Indeed, as with $Nup116^{CTD}$, complex formation is prevented by the $Nup82^{DFY}$ mutant, as well as by the corresponding K-loop mutations, $Nup100^{K910A}$, $Nup145N^{K558A}$, and $hNup98^{K814A}$ (Table 2).

In Vivo Analyses. In yeast, the deletion of Nup82 and Nup159 is lethal (6, 9–11), whereas that of Nup116 yields a temperature-sensitive phenotype (22). To test the physiological relevance of the interfaces that we have identified here, we analyzed haploid *S. cerevisiae* strains from which each of the three genes were deleted and replaced by various GFP-tagged wild-type and mutant constructs. The strains were then analyzed for growth and nuclear rim staining as an indicator for NPC incorporation.

For Nup82, deletion of its NTD, $Nup82^{\Delta NTD}$, yields growth defects with increasing temperatures (Fig. 6 *A* and *B*). While neither the $Nup82^{DFY}$ nor the $Nup82^{LILLF}$ mutants affected cell growth, their combination in $Nup82^{DFY-LILLF}$ mimicked the growth phenotype of the NTD deletion (Fig. 6 *A* and *B*). Likewise, detectable nuclear rim staining was observed only for the $Nup82^{DFY}$ or the $Nup82^{LILLF}$ mutants, but not for the $Nup82^{DFY-LILLF}$ or $Nup82^{\Delta NTD}$ mutants (Fig. 6*C*).

For Nup116 as well as for Nup159, the deletion of the crystallized domains from full-length proteins did not yield any detectable defect in either growth or nuclear rim localization (Figs. S7 and S8), indicating that these nucleoporins contain

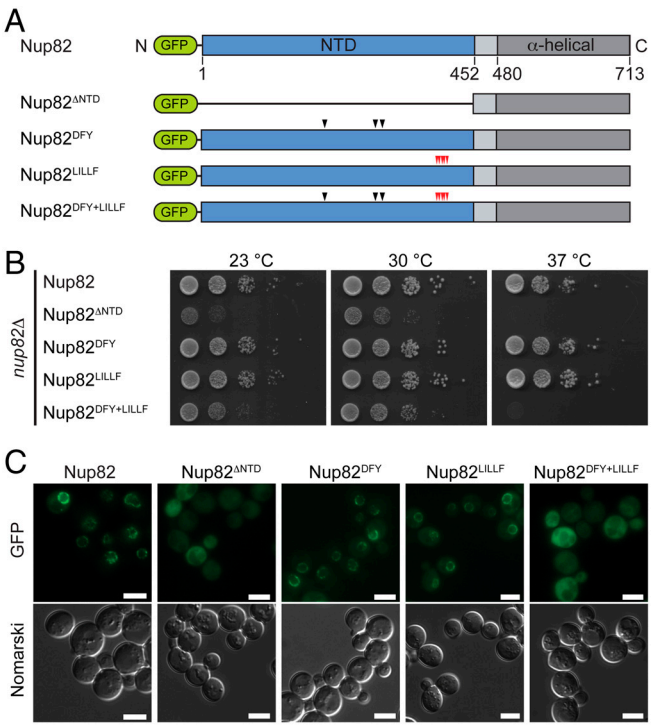

Fig. 6. In vivo analysis of Nup82 mutants. (*A*) Domain organization of the GFP-labeled Nup82 constructs, colored as in Fig. 1*A*. The black and red arrows indicate the positions of the DFY and LILLF mutations, respectively. (*B*) Yeast growth analysis using a *nup82*Δ strain transformed with the indicated GFP-Nup82 constructs. 10-fold serial dilutions were spotted on SD-Leu plates and grown for 2–3 d at the indicated temperatures. The combination of the DFY and LILLF mutations in one mutant ($Nup82^{DFY–LILLF}$) has the same effect on growth as the deletion of the entire NTD ($Nup82^{\Delta NTD}$). (*C*) In vivo localization of the GFP-Nup82 constructs at 37 °C. Both the $Nup82^{DFY–LILLF}$ and the $Nup82^{\Delta NTD}$ mutants fail to localize to the nuclear rim. The scale bars represent 5 μm.

additional domains for targeting to the NPC. In fact, for Nup116, we identified an additional upstream region (residues 686–967) that is involved in NPC targeting (Fig. S7*C*).

Discussion

We found that an N-terminal fragment comprising more than half of the Nup82 molecule folds into a β-propeller that serves as the binding platform for the C-terminal domain of Nup116 and the C-terminal tail of Nup159. For each of these interactions in the $Nup82^{NTD}$•$Nup159^{T}$•$Nup116^{CTD}$ heterotrimer, we identified hot-spot residues by mutational analyses and verified their critical nature by biochemical, biophysical, and in vivo experiments.

Equivalent domains of the yeast Nup116 paralogs, Nup100 and Nup145N, and the mammalian homolog, hNup98, bound to the Nup82 β-propeller in an evolutionarily conserved fashion and in a mutually exclusive manner. Of these, only Nup116 and hNup98 possess a binding site for Gle2 (or Rae1 or mrnp41) that functions in RNA export (5, 21–23). Hence, binding of either Nup116, Nup145N, or Nup100 could affect mRNA export. It is conceivable, for example, that replacement of yeast Nup116 by Nup100 or Nup145N in the M or S phase of the cell cycle, or during stationary growth, could coordinate reduced transcription with a slowdown of mRNA export.

Our in vivo targeting data show that the interaction sites in the heterotrimeric complex are not the only regions by which these nucleoporins are anchored to the NPC. For example, although the C-terminal domain of Nup116 yielded some nuclear rim staining, consistent with targeting to the NPC, we identified an additional targeting site upstream of the crystallized C-terminal domain. Likewise, after removal of the crystallized C-terminal tail of Nup159, the tailless Nup159 still displayed rim staining and showed only a slight accumulation in the cytoplasm, whereas a larger C-terminal truncation failed to target to the nuclear rim, as previously reported (8). For Nup82, the simultaneous mutational disruption of the two binding sites to Nup116 and Nup159 resulted in cytoplasmic localization with no detectable nuclear rim staining. However, rim staining was detected when only one of the binding sites was disrupted, suggesting that the loss of a single interaction can be tolerated. In addition to the two interactions described here, the C-terminal α-helical domain of Nup82 has previously been reported to interact with the α-helical region of the nucleoporin Nsp1 that is part of the transport channel in the core of the NPC (1, 24).

Taken together, our data indicate that Nup82 is a central interaction platform for the simultaneous binding of at least three nucleoporins, Nup116 (or their paralogs, Nup100 and Nup145N), Nup159, and Nsp1. The elucidation of the interactions in the $Nup82^{NTD}$•$Nup159^{T}$•$Nup116^{CTD}$ heterotrimer on the cytoplasmic face of the NPC is another substantial step toward a gradual reconstruction of the NPC at atomic resolution.

Methods

The details of protein expression, purification, crystallization, structure determination, protein interaction analysis, multiangle light scattering, and in vivo experiments are described in the *SI Text* published online. In short, DNA fragments of *S. cerevisiae* Nup82, Nup159, Nup100, Nup145N, Nup116, and human Nup98 were amplified by PCR and cloned into the vectors pET21a (Novagen), pETDuet-1 (Novagen), pET28a that was modified to contain an N-terminal PreScission protease cleavable His_6-tag, and pET28b that was modified to contain an N-terminal His_6-SUMO tag (25, 26). Point mutants were generated by QuikChange site-directed mutagenesis (Stratagene) and confirmed by DNA sequencing. Details of the bacterial expression constructs are listed in Table S1. All proteins were expressed in *Escherichia coli* using the appropriate expression constructs and purified using several chromatographic techniques. X-ray diffraction data were collected at the National Institute of General Medical Sciences and National Cancer Institute Collaborative Access Team (GM/CA-CAT) beamline at the Advanced Photon Source (APS), Argonne National Laboratory (ANL). The 5 μm "minibeam" collimator setup (27) was critical for obtaining excellent X-ray diffraction data from the twinned crystals. The structure was solved by SAD, using data obtained from selenomethionine-labeled crystals. Data collection and refinement statistics are summarized in Table 1.

ACKNOWLEDGMENTS. We thank Andrew Davenport for technical support; Alina Patke for discussions; David King (HHMI, UC Berkeley) for mass spectrometry analysis; Michael Becker, Robert Fischetti, Craig Ogata, and Ruslan Sanishvili (APS) for beamline support; the Biophysics Core Facility of the University of Colorado, Denver, for isothermal titration calorimetry. E.W.D. was supported by a Dale F. and Betty Ann Frey Fellowship of the Damon Runyon Cancer Research Foundation, DRG-1977-08, and A.H. by a SCOR grant from the Leukemia and Lymphoma Society.

1. Hoelz A, Debler EW, Blobel G (2011) The structure of the nuclear pore complex. *Annu Rev Biochem* 80:613–643.
2. Beck M, Lucic V, Forster F, Baumeister W, Medalia O (2007) Snapshots of nuclear pore complexes in action captured by cryo-electron tomography. *Nature* 449:611–615.
3. Radu A, Moore MS, Blobel G (1995) The peptide repeat domain of nucleoporin Nup98 functions as a docking site in transport across the nuclear pore complex. *Cell* 81:215–254.
4. Cook A, Bono F, Jinek M, Conti E (2007) Structural biology of nucleocytoplasmic transport. *Annu Rev Biochem* 76:647–671.
5. Wente SR, Rout MP, Blobel G (1992) A new family of yeast nuclear pore complex proteins. *J Cell Biol* 119:705–723.
6. Hurwitz ME, Blobel G (1995) NUP82 is an essential yeast nucleoporin required for poly (A)+ RNA export. *J Cell Biol* 130:1275–1281.
7. Hurwitz ME, Strambio-de-Castillia C, Blobel G (1998) Two yeast nuclear pore complex proteins involved in mRNA export form a cytoplasmically oriented subcomplex. *Proc Natl Acad Sci USA* 95:11241–11245.
8. Del Priore V, et al. (1997) A structure/function analysis of Rat7p/Nup159p, an essential nucleoporin of *Saccharomyces cerevisiae*. *J Cell Sci* 110:2987–2999.
9. Grandi P, et al. (1995) A novel nuclear pore protein Nup82p which specifically binds to a fraction of Nsp1p. *J Cell Biol* 130:1263–1273.
10. Gorsch LC, Dockendorff TC, Cole CN (1995) A conditional allele of the novel repeat-containing yeast nucleoporin RAT7/NUP159 causes both rapid cessation of mRNA export and reversible clustering of nuclear pore complexes. *J Cell Biol* 129:939–955.
11. Kraemer DM, Strambio-de-Castillia C, Blobel G, Rout MP (1995) The essential yeast nucleoporin NUP159 is located on the cytoplasmic side of the nuclear pore complex and serves in karyopherin-mediated binding of transport substrate. *J Biol Chem* 270:19017–19021.
12. Stelter P, et al. (2007) Molecular basis for the functional interaction of dynein light chain with the nuclear-pore complex. *Nat Cell Biol* 9:788–796.
13. Ho AK, et al. (2000) Assembly and preferential localization of Nup116p on the cytoplasmic face of the nuclear pore complex by interaction with Nup82p. *Mol Cell Biol* 20:5736–5748.
14. Robinson MA, et al. (2005) Multiple conformations in the ligand-binding site of the yeast nuclear pore-targeting domain of Nup116p. *J Biol Chem* 280:35723–35732.
15. Paoli M (2001) Protein folds propelled by diversity. *Prog Biophys Mol Biol* 76:103–130.
16. Hodel AE, et al. (2002) The three-dimensional structure of the autoproteolytic, nuclear pore-targeting domain of the human nucleoporin Nup98. *Mol Cell* 10:347–358.
17. Sampathkumar P, et al. (2010) Structures of the autoproteolytic domain from the *Saccharomyces cerevisiae* nuclear pore complex component, Nup145. *Proteins* 78:1992–1998.
18. Rosenblum JS, Blobel G (1999) Autoproteolysis in nucleoporin biogenesis. *Proc Natl Acad Sci USA* 96:11370–11375.
19. Fontoura BM, Blobel G, Matunis MJ (1999) A conserved biogenesis pathway for nucleoporins: proteolytic processing of a 186-kilodalton precursor generates Nup98 and the novel nucleoporin, Nup96. *J Cell Biol* 144:1097–1112.
20. Teixeira MT, et al. (1997) Two functionally distinct domains generated by in vivo cleavage of Nup145p: a novel biogenesis pathway for nucleoporins. *EMBO J* 16:5086–5097.
21. Bailer SM, et al. (1998) Nup116p and nup100p are interchangeable through a conserved motif which constitutes a docking site for the mRNA transport factor gle2p. *EMBO J* 17:1107–1119.
22. Wente S, Blobel G (1993) A temperature-sensitive *NUP116* null mutant forms a nuclear envelope seal over the yeast nuclear pore complex thereby blocking nucleocytoplasmic traffic. *J Cell Biol* 123:275–284.
23. Ren Y, Seo HS, Blobel G, Hoelz A (2010) Structural and functional analysis of the interaction between the nucleoporin Nup98 and the mRNA export factor Rae1. *Proc Natl Acad Sci USA* 107:10406–10411.
24. Bailer SM, Balduf C, Hurt E (2001) The Nsp1p carboxy-terminal domain is organized into functionally distinct coiled-coil regions required for assembly of nucleoporin subcomplexes and nucleocytoplasmic transport. *Mol Cell Biol* 21:7944–7955.
25. Hoelz A, Nairn AC, Kuriyan J (2003) Crystal structure of a tetradecameric assembly of the association domain of Ca2+/calmodulin-dependent kinase II. *Mol Cell* 11:1241–1251.
26. Mossessova E, Lima CD (2000) Ulp1-SUMO crystal structure and genetic analysis reveal conserved interactions and a regulatory element essential for cell growth in yeast. *Mol Cell* 5:865–876.
27. Fischetti RF, et al. (2009) Mini-beam collimator enables microcrystallography experiments on standard beamlines. *J Synchrotron Radiat* 16:217–225.
28. Laskowski RA, MacArthur MW, Moss DS, Thornton JM (1993) PROCHECK—a program to check the stereochemical quality of protein structures. *J App Crystallogr* 26:283–291.